nature immunology

ARTICLES

https://doi.org/10.1038/s41590-019-0515-x

Fibroblastic reticular cells enhance T cell metabolism and survival via epigenetic remodeling

Flavian D. Brown[1,2,3,4,5,13], Debattama R. Sen[1,2], Martin W. LaFleur[1,2,3,4], Jernej Godec[1,2,3,4], Veronika Lukacs-Kornek[5,14], Frank A. Schildberg[3,4,5,15], Hye-Jung Kim[3,5], Kathleen B. Yates[2,6], Stéphane J. H. Ricoult[7], Kevin Bi[2,6], Justin D. Trombley[3,4], Varun N. Kapoor[8], Illana A. Stanley[9,10], Viviana Cremasco[5,16], Nika N. Danial[9,10], Brendan D. Manning[7], Arlene H. Sharpe[3,4,6,11*], W. Nicholas Haining[2,6,12,17*] and Shannon J. Turley[5,8*]

Lymph node fibroblastic reticular cells (FRCs) respond to signals from activated T cells by releasing nitric oxide, which inhibits T cell proliferation and restricts the size of the expanding T cell pool. Whether interactions with FRCs also support the function or differentiation of activated CD8$^+$ T cells is not known. Here we report that encounters with FRCs enhanced cytokine production and remodeled chromatin accessibility in newly activated CD8$^+$ T cells via interleukin-6. These epigenetic changes facilitated metabolic reprogramming and amplified the activity of pro-survival pathways through differential transcription factor activity. Accordingly, FRC conditioning significantly enhanced the persistence of virus-specific CD8$^+$ T cells in vivo and augmented their differentiation into tissue-resident memory T cells. Our study demonstrates that FRCs play a role beyond restricting T cell expansion—they can also shape the fate and function of CD8$^+$ T cells.

Lymph nodes (LNs) contain hematopoietic cell lineages and several specialized stromal cells, including blood endothelial cells, lymphatic endothelial cells, follicular dendritic cells, marginal reticular cells, integrin α_7^+ pericytes and fibroblastic reticular cells (FRCs)[1–5]. LN stromal cells have primarily been viewed as structural determinants, uninvolved in immune cell homeostasis or ongoing immune responses. However, a series of recent publications has uncovered several immunoregulatory properties of LN stromal cells. In particular, T cell zone FRCs are concentrated in the paracortical region (T cell zone) of the LN and are endowed with functions that regulate the activity of T lymphocytes[6–11]. FRCs express the lymphocyte chemoattractants CCL19 and CCL21, which function to support naïve T cell trafficking across high endothelial venules and retain T cells in the LN paracortex through their ligation to CCR7 (refs. [4,12–16]). In addition to migration, FRCs support naïve T cell homeostasis by expressing interleukin-7 (IL-7) and aid T cell priming by facilitating interactions between T cells and antigen-presenting dendritic cells[13,17–19]. During T cell priming, the FRC network elongates in response to signals from antigen-bearing dendritic cells—which allows space for T cell influx and clonal expansion[20,21].

Although the FRC network relaxes to facilitate an area for T cell expansion, direct signals from FRCs actively restrict and curtail proliferation of the expanding T cell pool. Multiple studies have shown that FRCs and activated T cells engage in a molecular cross-talk whereby T cell-derived interferon-γ (IFN-γ) and tumor necrosis factor (TNF) act synergistically to enable FRCs with suppressive capabilities that are mediated through the activity of inducible nitric oxide synthase (NOS2)[22–24]. However, only a portion of FRCs expressed NOS2 in vivo during T cell priming[22,23]. These data indicate that FRCs may have a functional role beyond restricting T cell expansion. Indeed, recent publications have described the functional diversity of LN FRCs given their ability to regulate B and plasma cell homeostasis[25–27]. These studies highlighted the pleiotropic nature of FRCs, thus raising the possibility of their functional heterogeneity also within the T cell zone. Therefore, whether FRCs can enhance the function or support the differentiation of newly activated CD8$^+$ T cells remains an open question.

Here we report a previously unrecognized function of LN FRCs during T cell activation. In response to signals from activated T cells, FRCs upregulated molecules with immunostimulatory function—namely ICOS ligand (ICOSL), CD40 and interleukin-6 (IL-6). Once released from FRCs, IL-6 enhanced IL-2 and TNF production by activated CD8$^+$ T cells. FRC-derived signals, including IL-6, led to chromatin remodeling in activated CD8$^+$ T cells, which promoted the expression of genes involved in bioenergetic and pro-survival

[1]Division of Medical Sciences, Harvard Medical School, Boston, MA, USA. [2]Department of Pediatric Oncology, Dana-Farber Cancer Institute, Boston, MA, USA. [3]Department of Microbiology and Immunobiology, Harvard Medical School, Boston, MA, USA. [4]Evergrande Center for Immunologic Diseases, Harvard Medical School and Brigham and Women's Hospital, Boston, MA, USA. [5]Department of Cancer Immunology and Virology, Dana-Farber Cancer Institute, Boston, MA, USA. [6]Broad Institute of Harvard and Massachusetts Institute of Technology, Cambridge, MA, USA. [7]Department of Genetics and Complex Diseases, Harvard T.H. Chan School of Public Health, Boston, MA, USA. [8]Department of Cancer Immunology, Genentech, South San Francisco, CA, USA. [9]Department of Cancer Biology, Dana-Farber Cancer Institute, Boston, MA, USA. [10]Department of Cell Biology, Harvard Medical School, Boston, MA, USA. [11]Department of Pathology, Brigham and Women's Hospital, Boston, MA, USA. [12]Division of Pediatric Hematology and Oncology, Children's Hospital, Boston, MA, USA. [13]Present address: Neon Therapeutics Inc., Cambridge, MA, USA. [14]Present address: Institute of Experimental Immunology, University Hospital of the Rheinische Friedrich-Wilhelms-University, Bonn, Germany. [15]Present address: Clinic for Orthopedics and Trauma Surgery, University Hospital Bonn, Bonn, Germany. [16]Present address: Immuno-Oncology, Novartis Institutes for BioMedical Research, Cambridge, MA, USA. [17]Present address: Merck Research Laboratories, Boston, MA, USA. *e-mail: arlene_sharpe@hms.harvard.edu; nick.haining@merck.com; turley.shannon@gene.com

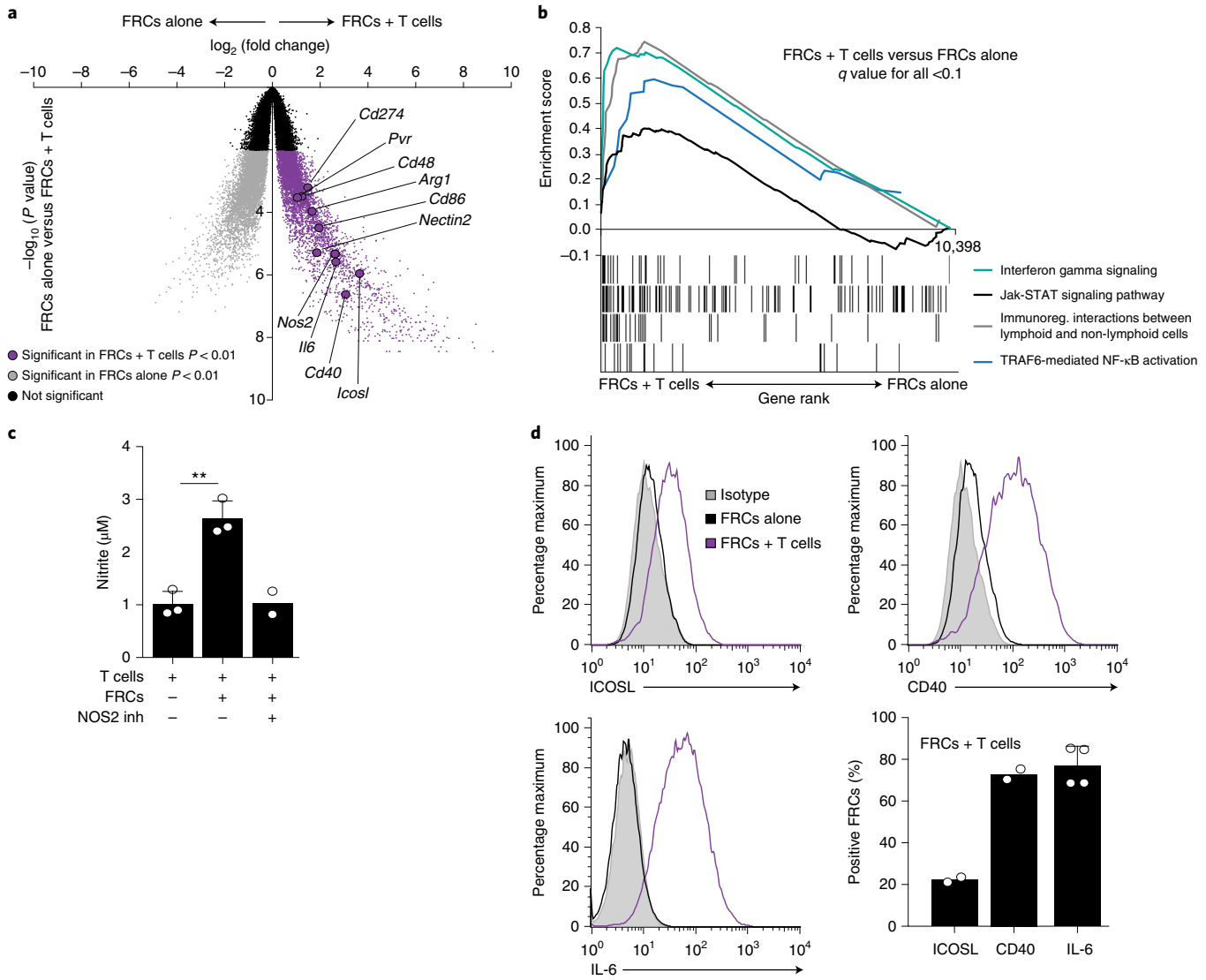

Fig. 1 | FRCs upregulate both immunosuppressive and stimulatory molecules in response to activated T cells. a, Volcano plot of transcriptional probes upregulated in resting FRCs (gray, $P < 0.01$, linear modeling and empirical Bayesian method, limma) or FRCs co-cultured for 16 h with whole splenocytes activated with anti-CD3/CD28 (purple, $P < 0.01$, linear modeling and empirical Bayesian method, limma) ($n = 2$ biologically independent cell cultures). **b**, Gene set enrichment analysis[58,59] of MSigDB signatures significantly upregulated in FRCs co-cultured for 16 h with activated splenocytes (FRCs + T cells, $P < 0.05$, $q < 0.1$) versus resting FRCs (FRCs alone) ($n = 2$ biologically independent cell cultures). Jak-STAT, Janus kinase (Jak)-signal transducer of activators of transscription (STAT); NF-κB, nuclear factor-κB; TRAF6, tumor necrosis factor receptor–associated factor 6 (TRAF6). **c**, Nitric oxide production in supernatants of splenocytes activated with anti-CD3/CD28 alone (T cells), in the presence of WT FRCs (FRCs) or in the presence of WT FRCs and inhibitor L-NMMA (NOS2 inh) ($n = 3$ (T cells and FRCs) and 2 (NOS2 inh) biologically independent cell cultures). $^{**}P = 0.0025$ (two-tailed Student's *t*-test). **d**, Surface staining of ICOSL (top left) and CD40 (top right) and ICS of IL-6 (bottom left) in resting FRCs and FRCs co-cultured for 24 h with activated splenocytes. The histograms are representative plots; bar graph (bottom right) summarizes the percentage of FRCs that are positive for each molecule following their co-culture with activated T cells. $n = 2$ biologically independent cell cultures (ICOSL and CD40) and 4 biologically independent cell cultures (IL-6). Data in **a**,**b** represent one experiment. Data in **c** are representative of two biologically independent experiments (mean ± s.d.). Data in **d** are the composite of two biologically independent experiments (mean ± s.d.).

pathways. In vivo, FRC-conditioned T cells persisted significantly longer following adoptive transfer into virally infected animals and preferentially differentiated into tissue-resident memory T (TRM) cells. These data demonstrate that LN FRCs, which are closely positioned near T cells during priming, can transmit long-lasting signals into activated $CD8^+$ T cells to support their function, survival and differentiation.

Results

FRCs can express functionally diverse molecules. To investigate whether FRCs express molecules capable of promoting the functions of activated T cells, we expanded FRCs from primary LN stromal cell cultures as previously described[22], and then cultured them alone or with splenocytes activated with soluble antibody against CD3 and CD28 (hereafter anti-CD3/CD28) for 16 h. We generated transcriptional profiles of FRCs from each condition and found that FRCs co-cultured with activated splenocytes significantly upregulated 2,390 genes compared to their resting counterparts ($P < 0.01$) (Fig. 1a). Expected gene signatures induced by T cell-derived cytokines, such as IFN-γ, were significantly enriched in FRCs following exposure to activated T cells ($q < 0.1$) (Fig. 1b). Expression analysis of individual genes confirmed previous findings but also uncovered

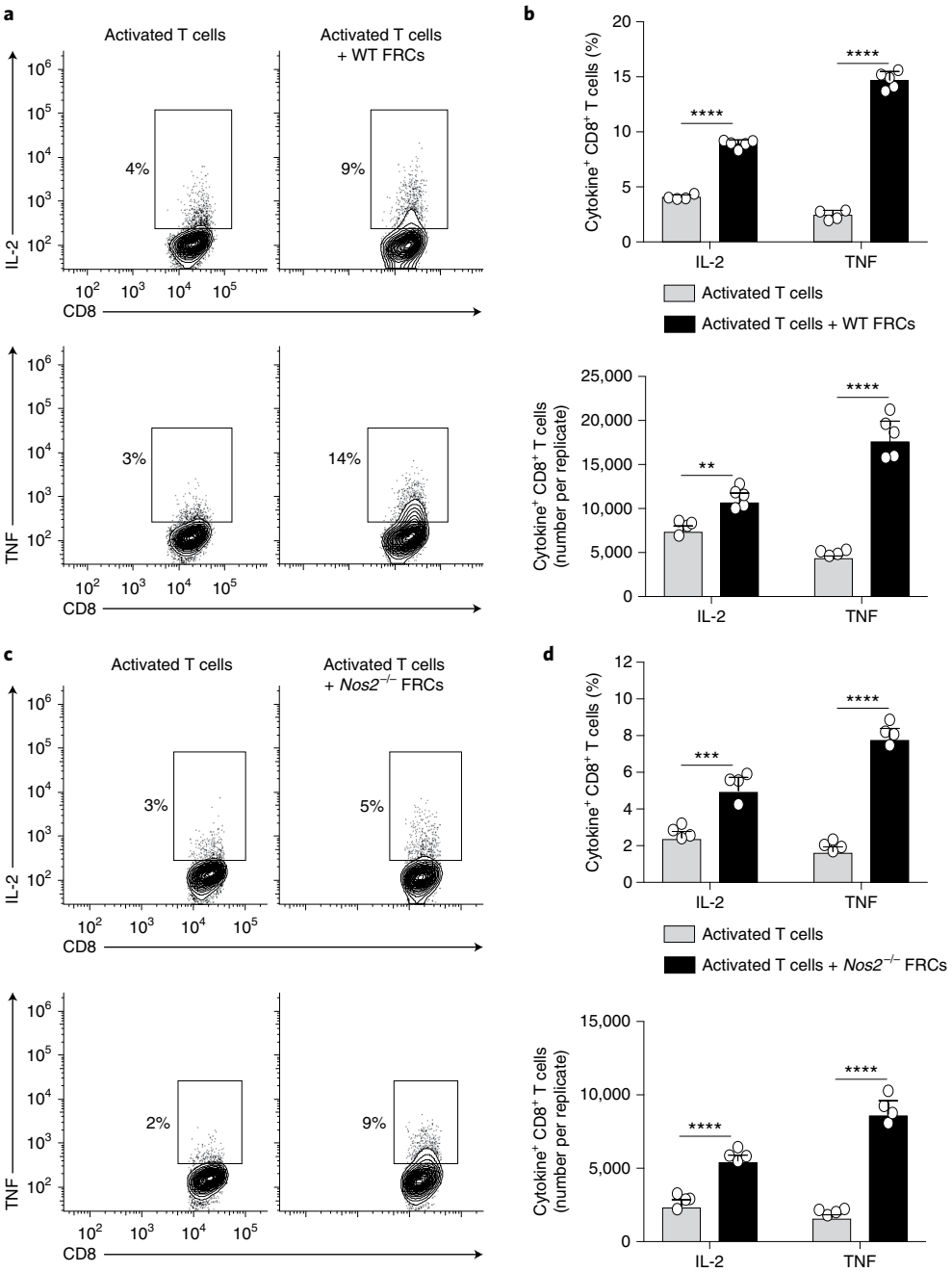

Fig. 2 | FRCs enhance CD8⁺ T cell cytokine production independently of Nos2 expression. a, ICS for IL-2 (top) and TNF (bottom) in CD8⁺ T cells activated either in splenocyte mixtures via anti-CD3/CD28 for 24 h or via anti-CD3/CD28 for 24 h in the presence of WT FRCs. **b**, Summary of results in **a** as percentage of cytokine-positive cells (top) ($n = 4$ (activated T cells) and 5 (activated T cells + WT FRCs) biologically independent cell cultures per group) and as absolute number of cytokine-positive cells (bottom). $^{**}P = 0.0014$, $^{****}P < 0.0001$ (two-tailed Student's *t*-test). **c**, Repeat of ICS experimental design in **a** using *Nos2*$^{-/-}$ FRCs. **d**, Summary of results in **c** as percentage of cytokine-positive cells (top) ($n = 4$ (activated T cells) and 4 (activated T cells + *Nos2*$^{-/-}$ FRCs) biologically independent cell cultures per group) and as absolute number of cytokine-positive cells (bottom). $^{***}P = 0.0007$, $^{****}P < 0.0001$ (two-tailed Student's *t*-test). Data in **b** and **d** are a composite of two biologically independent experiments (mean ± s.d.).

some unanticipated results. Consistent with published reports[22–24], FRCs upregulated expression of genes encoding molecules known to dampen T cell function, such as *Arg1*, *Cd274* and *Nos2* (Fig. 1a,c). However, FRCs also upregulated molecules with immunostimulatory capabilities in response to activated T cells. We detected increased expression of *Icosl*, *Cd40* and *Il6* in FRCs co-cultured with activated T cells (Fig. 1a). We validated these findings by comparing ICOSL, CD40 and IL-6 protein expression in resting FRCs versus FRCs co-cultured with activated T cells. Flow cytometric analyses revealed a robust increase in ICOSL, CD40 and IL-6 in FRCs co-cultured with activated T cells at 24 h (Fig. 1d). These results suggest that FRCs may exhibit some functional duality in regard to their ability to regulate T cell biology, since they can express molecules that suppress and enhance T cell functions.

FRCs use IL-6 to regulate cytokine production by T cells. Given their expression of molecules known to positively influence T cell function, we asked whether FRCs could enhance the production

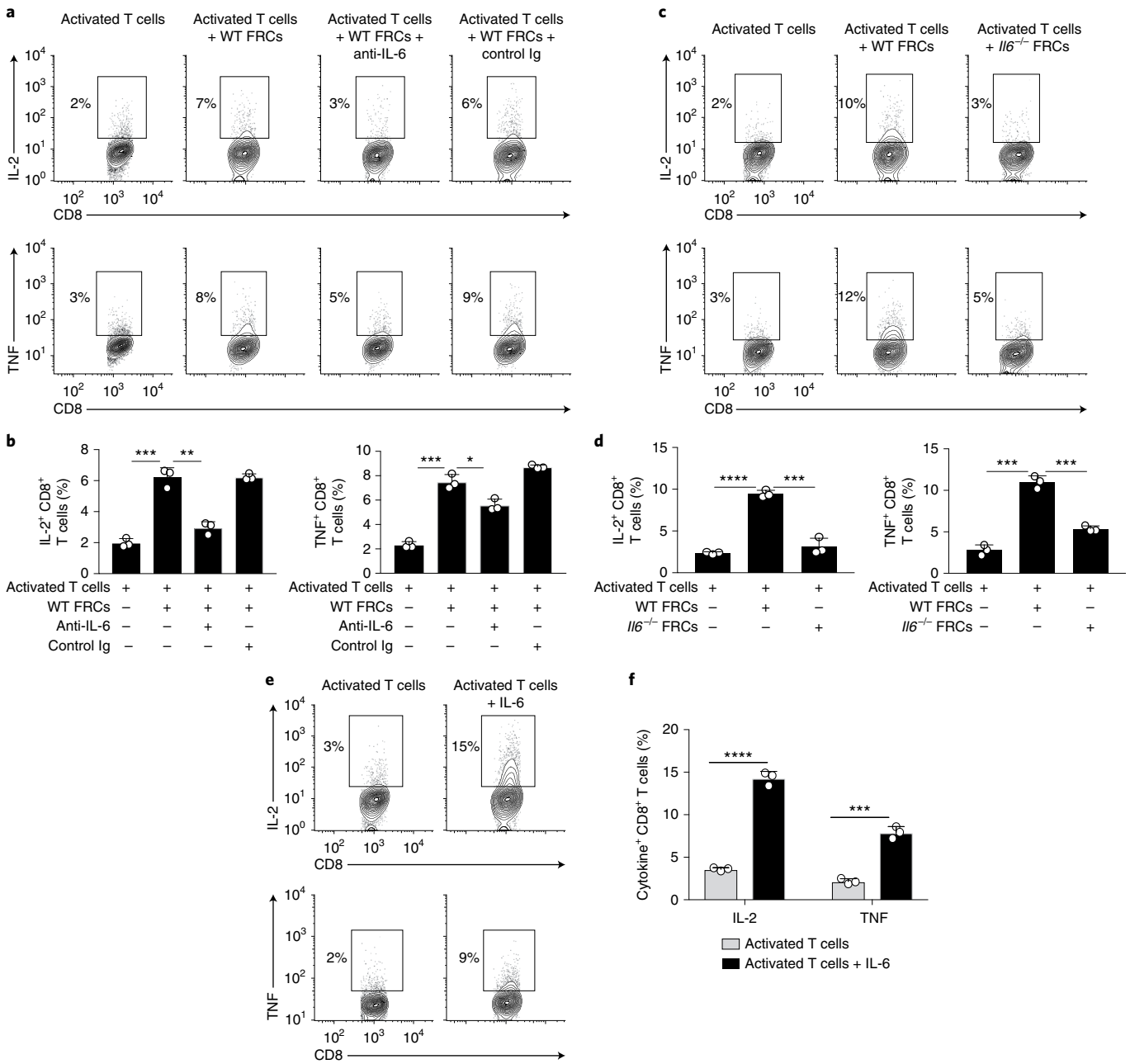

Fig. 3 | FRC-derived IL-6 is necessary and sufficient for the enhanced production of CD8⁺ T cell cytokines. a, ICS for IL-2 (top) and TNF (bottom) in CD8⁺ T cells activated in whole-splenocyte mixtures via anti-CD3/CD28 for 24 h (Act), activated via anti-CD3/CD28 in the presence of WT FRCs (WT FRCs), 1 μg ml^{-1} anti-IL-6 blocking antibody or 1 μg ml^{-1} isotype control antibody. **b**, Summary of results in **a** ($n = 3$ biologically independent cell cultures per group). *$P = 0.0133$, **$P = 0.0015$, ***$P = 0.0004$ (Act versus WT FRCs–IL-2), ***$P = 0.0002$ (Act versus WT FRCs–TNF) (two-tailed Student's *t*-test). **c**, Repeat of ICS experimental design in **a** using *Il6*$^{-/-}$ FRCs. **d**, Summary of results in **c** ($n = 3$ biologically independent cell cultures per group). ***$P = 0.0005$ (WT FRCs versus *Il6*$^{-/-}$ FRCs–IL-2), ***$P = 0.0001$ (Act versus WT FRCs–TNF), ***$P = 0.0003$ (WT FRCs versus *Il6*$^{-/-}$ FRCs–TNF), ****$P < 0.0001$ (two-tailed Student's *t*-test). **e**, ICS for IL-2 (top) and TNF (bottom) in CD8⁺ T cells activated either within whole-splenocyte mixtures via anti-CD3/CD28 for 24 h or with anti-CD3/CD28 plus 100 ng ml^{-1} recombinant IL-6. **f**, Summary of results in **e** ($n = 3$ biologically independent cell cultures per group) ***$P = 0.0002$, ****$P < 0.0001$ (two-tailed Student's *t*-test). Data are representative of two biologically independent experiments (mean ± s.d.).

of cytokines in newly activated CD8⁺ T cells. In a previous study, CD8⁺ T cells activated in the presence of FRCs produced less IFN-γ compared to T cells activated alone[23]. It is important to note that this study measured cytokine production at a time point (96 h post activation) that compared proliferating T cells to those experiencing proliferative disruption by nitric oxide. To unmask any stimulatory activity of FRCs independent of the inhibition mediated by nitric oxide, we performed intracellular staining (ICS) at a time point (24 h post activation) that precedes the release of nitric oxide by FRCs. Similar to previous studies, we also found that signals from FRCs dampened IFN-γ production in newly activated T cells (Supplementary Fig. 1b,c). The production of IL-2 and TNF, however, was significantly elevated in activated CD8⁺ T cells co-cultured with FRCs (Fig. 2a,b). To determine whether FRC-mediated stimulation requires the involvement of accessory cells, we conducted the assay with purified CD8⁺ T cells rather than unfractionated

splenocytes. The degree of stimulation by FRCs cultured alone with T cells was similar to that of co-cultures involving splenocytes—indicating direct stimulation of T cells by FRCs (Supplementary Fig. 1d,e). To rule out the potential effects of trace amounts of nitric oxide in the co-cultures, we repeated the experiment with *Nos2*$^{-/-}$ FRCs. Interestingly, CD8$^+$ T cells activated in the presence of *Nos2*$^{-/-}$ FRCs also produced significantly higher amounts of IL-2 and TNF compared to CD8$^+$ T cells activated without FRCs (Fig. 2c,d). These results demonstrate that FRCs enhance IL-2 and TNF production by CD8$^+$ T cells independent of NOS2 expression.

We next assessed the relative roles of several FRC-derived molecules in enhancing IL-2 and TNF production by CD8$^+$ T cells, and found the most significant impact when targeting the activity of IL-6. Blocking antibody against IL-6 significantly attenuated the increased production of IL-2 and TNF by CD8$^+$ T cells activated in the presence of FRCs (Fig. 3a,b), suggesting that FRCs use IL-6 to boost the production of T cell cytokines. Indeed, CD8$^+$ T cells activated in the presence of *Il6*$^{-/-}$ FRCs produced significantly less IL-2 and TNF compared to CD8$^+$ T cells activated in the presence of wild-type (WT) FRCs (Fig. 3c,d). Consistent with these findings, supplementation of our cultures with recombinant IL-6 significantly augmented IL-2 and TNF production in activated CD8$^+$ T cells (Fig. 3e,f). Thus, IL-6 produced by FRCs is both necessary and sufficient for the enhanced production of cytokines by newly activated CD8$^+$ T cells.

FRCs remodel the transcriptome and epigenome of T cells. The profound impact of FRCs on early T cell cytokine production prompted us to ask whether FRC signals enhance additional aspects of CD8$^+$ T cell function. To address this question broadly, we profiled the epigenetic and transcriptional state of CD8$^+$ T cells activated in vitro for 48 h with anti-CD3/CD28 (Act), with or without recombinant IL-6 (Act + IL-6) or activated with anti-CD3/CD28 in the presence of FRCs (Act + FRCs). Given the equivalent capacity of WT and *Nos2*$^{-/-}$ FRCs to enhance T cell cytokine production, we used *Nos2*$^{-/-}$ FRCs for our profiling and subsequent studies. This experimental design allowed us to profile T cells with comparable activation status and proliferative capacities (Supplementary Fig. 2), while avoiding additional nitric oxide-induced deleterious effects such as mitochondrial inhibition and DNA damage[28,29].

We used an assay for transposase-accessible chromatin with high-throughput sequencing (ATAC-seq)[30] to identify 81,821 high-quality (Supplementary Fig. 3a–d) chromatin-accessible regions (ChARs) in activated CD8$^+$ T cells in all three conditions ($q < 0.001$). Hierarchical clustering of replicates by condition based on Pearson correlation revealed that activated CD8$^+$ T cells conditioned with FRCs or IL-6 were more similar in their global pattern of chromatin accessibility than those activated in the absence of FRCs or IL-6 (Fig. 4a). Further analysis suggested that the similarity between the epigenetic state of activated CD8$^+$ T cells co-cultured with FRCs or IL-6 was driven by a greater number of shared ChARs (6,145), compared to cells activated with only anti-CD3/CD28 (2,614 and 3,670, respectively) (Fig. 4b). Differential accessibility analysis further supported the similarity between activated CD8$^+$ T cells exposed to signals from FRCs or IL-6. Compared to T cells activated alone, signals from FRCs significantly induced greater accessibility at 402 ChARs ($q < 1 \times 10^{-40}$; DESeq2) (Fig. 4c). Strikingly, 100% of these FRC-responsive regions were also more open in CD8$^+$ T cells cultured with IL-6 compared to those activated alone (Fig. 4d). Unsupervised clustering of differential ChARs identified four characteristic 'modules' of chromatin accessibility across the three T cell states. Notably, one of those modules represented a shared cluster of differential regions present in both FRC and IL-6 conditions (module 4) (Fig. 4e). Taken together, these analyses suggest that signals from FRCs and IL-6 reorganize accessible chromatin in activated CD8$^+$ T cells in a similar manner—which is markedly distinct from the epigenetic state induced by anti-CD3/CD28 activation alone.

Analysis of transcriptional profiles (Supplementary Fig. 3e–g) also revealed marked similarities between CD8$^+$ T cells activated in the presence of FRCs or IL-6 versus T cells solely receiving anti-CD3/CD28 activation. FRC-derived factors led to the upregulation of 778 genes in CD8$^+$ T cells compared to those receiving baseline activation ($q < 1 \times 10^{-10}$; DESeq2) (Fig. 4f). Notably, 76% of these FRC-responsive genes were also upregulated in CD8$^+$ T cells cultured with IL-6 relative to their activity in CD8$^+$ T cells exclusively activated by anti-CD3/CD28 (Fig. 4g). Thus, genes that are significantly upregulated in response to FRC-derived factors also tend to be differentially expressed in response to IL-6. Additionally, we found a positive correlation between the average peak intensity of ChARs within each ATAC-seq-defined module and the average gene expression of neighboring genes (Fig. 4e,h). This result implies that, on average, the ChARs within each module tend to positively regulate, rather than suppress, target genes. When compared to baseline anti-CD3/CD28 activation, these results suggest that signals from FRCs and IL-6 mediate changes through a shared set of enhancers in activated CD8$^+$ T cells that regulate distinct patterns of gene expression.

FRCs influence T cell metabolism, survival and memory. We next sought to further characterize the shared regulation of CD8$^+$ T cell enhancer activity and gene expression induced by FRC- and IL-6-derived signals. Gene Ontology term enrichment analysis within each ATAC-seq module revealed enrichment of pathways essential for CD8$^+$ T cell activation, survival and differentiation (Fig. 5a). In particular, we found marked enhancement of metabolic terms within the shared FRC/IL-6 module (module 4) (Fig. 5a). Although T cells are known to undergo substantial changes in energy consumption and utilization following activation[31–33], enrichment of

Fig. 4 | FRCs or IL-6 alter enhancers in activated CD8$^+$ T cells that regulate distinct patterns of gene expression. a, Display of chromatin-accessible regions (ChARs) using hierarchical clustering of replicates by condition with Pearson correlation. The conditions were CD8$^+$ T cells sorted following activation in whole-splenocyte mixtures via soluble anti-CD3/CD28 for 48 h (Act), activated with anti-CD3/CD28 in the presence of *Nos2*$^{-/-}$ FRCs (Act + FRC) or activated with anti-CD3/CD28 plus 100 ng ml^{-1} recombinant IL-6 (Act + IL-6) ($n = 3$ biologically independent cell cultures). **b**, Quantification of shared ChARs between each condition ($q \leq 0.001$, MACS2 (Poisson distribution and Benjamini–Hochberg correction)) ($n = 3$ biologically independent cell cultures). **c**, Volcano plot highlighting differential chromatin accessibility in CD8$^+$ T cells from Act condition (gray, $q < 1 \times 10^{-40}$, DESeq2) versus CD8$^+$ T cells from FRC condition (purple, $q < 1 \times 10^{-40}$, DESeq2) ($n = 3$ biologically independent cell cultures). **d**, Reprojection of FRC-responsive ChARs from **c** onto volcano plots comparing Act versus Act + IL-6 condition ($n = 3$ biologically independent cell cultures). **e**, Heat map with unsupervised clustering of differential ChARs across each condition ($n = 3$ biologically independent cell cultures). **f**, Volcano plot highlighting differential transcripts present in CD8$^+$ T cells from Act condition (gray, $q < 1 \times 10^{-10}$, DESeq2) versus CD8$^+$ T cells from FRC condition (teal, $q < 1 \times 10^{-10}$, DESeq2) ($n = 3$ biologically independent cell cultures (FRC) and 2 biologically independent cell cultures (Act)). **g**, Reprojection of FRC-responsive transcripts from **f** onto volcano plots comparing Act versus Act + IL-6 condition ($n = 2$ biologically independent cell cultures for each condition). **h**, Heat map correlating average peak intensity of ChARs in **e** and the average gene expression of neighboring genes ($n = 3$ biologically independent cell cultures (FRC) and 2 biologically independent cell cultures (Act and IL-6)). Data represent one ATAC-seq and one RNA-seq experiment.

these terms specifically in module 4 implies that signals from FRCs or IL-6 may further amplify or differentially alter the metabolic reprogramming that occurs in CD8+ T cells following activation.

We performed motif enrichment analysis to identify differential accessibility of specific TF binding motifs in each T cell condition. Compared to motifs accessible following baseline anti-CD3/CD28 activation, signals from FRCs significantly increased the accessibility of binding motifs for MYC ($P = 1.27 \times 10^{-9}$), HIF-1α ($P = 1.48 \times 10^{-6}$) and HIF-1β ($P = 0.0008$)—which are known to initiate and maintain the activity of metabolic pathways following T cell activation (Fig. 5b)[34–36]. FRC-derived factors also induced the enrichment of TF binding motifs essential for CD8+ T cell survival and memory differentiation, such as BATF, ETS1 and BACH2 (Fig. 5b)[37–40]. Compared to baseline anti-CD3/CD28 activation,

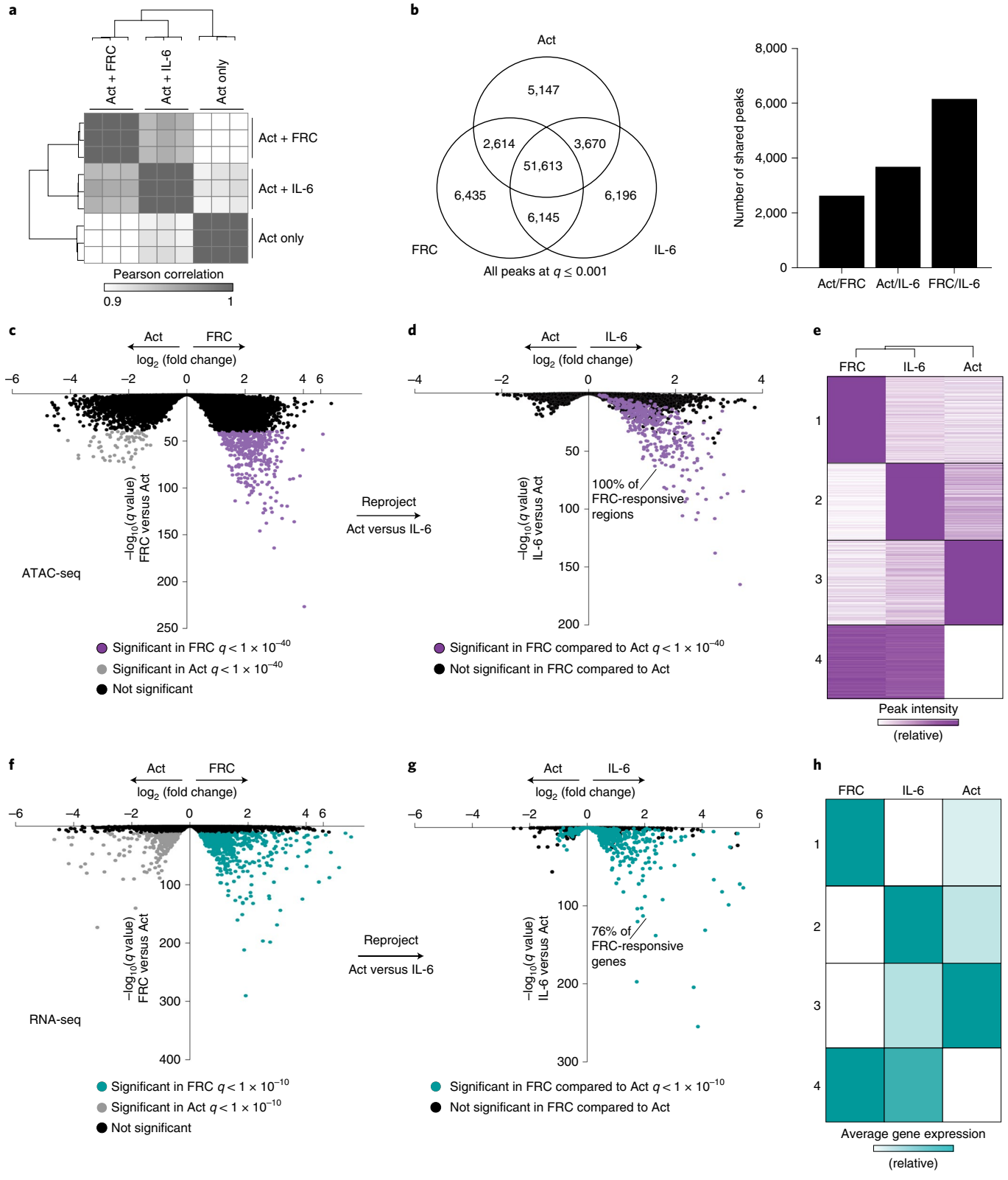

binding motifs for 32 TFs, including MYC, BATF and BACH2, were significantly enriched in both FRC and IL-6 conditions (Fig. 5c). To determine whether FRC-mediated changes in ChARs overlap with epigenetic profiles observed in memory cells, we compared our ATAC-seq profiles to H3K4me3 ChIP-seq profiles of naïve, terminal effector and memory precursor cells[41]. Compared to the baseline anti-CD3/CD28 condition, which enriches for neither the terminal effector nor memory precursor landscape, our analysis suggested that regions induced by either FRCs or IL-6 stimulation, but not both, were generally associated with a terminal effector phenotype (Supplementary Fig. 3h). Notably, ChARs that are instead induced by both FRC and IL-6 conditioning were significantly enriched for memory precursor-specific epigenetic modifications ($P = 8.3722 \times 10^{-7}$, hypergeometric test; Supplementary Fig. 3h). Consistent with these results, ChARs shared between FRC-conditioned and IL-6-stimulated cells showed marked similarity to CD8$^+$ memory T cells responding to acute lymphocytic choriomeningitis virus (LCMV) infection[42] ($P = 2.9561 \times 10^{-166}$, hypergeometric test; Supplementary Fig. 3i).

Inspection of ChARs surrounding genes central to glycolytic metabolism (*Hk1* and *Pfkfb3*) and pro-survival (*Bcl2* and *Cflar*) revealed significantly enhanced accessibility in CD8$^+$ T cells cultured with FRCs or IL-6 compared to cells receiving anti-CD3/CD28 activation ($q < 0.001$) (Fig. 5d,f). This differential accessibility was concordant with gene expression for MYC- and HIF-1-dependent glycolytic genes[34,36] (Fig. 5e) and vital pro-survival genes[43] (encoding BCL-2 family members, inhibitors of apoptosis members and *Cflar*) (Fig. 5g). Altogether, these results suggest that signals from FRCs or IL-6 induce epigenetic remodeling that promotes pathways associated with metabolic reprogramming, T cell longevity and memory cell differentiation.

FRCs elevate the bioenergetics of activated CD8$^+$ T cells. To validate the findings from the ATAC-seq and RNA-seq studies, we assessed the biochemical activity of essential metabolic pathways in CD8$^+$ T cells cultured under each condition. Following T cell antigen receptor (TCR) ligation and binding of co-stimulatory molecules, naïve T cells undergo major metabolic reprogramming—shifting away from metabolic quiescence to become predominantly reliant on aerobic glycolysis to fuel biomass accumulation and proliferation[31]. This switch to glycolysis occurs through the increased expression of nutrient transporters and via the activation of the key metabolic regulator, mechanistic target of rapamycin (mTOR)[31]. To analyze the activity of mTOR, we used phospho flow cytometry to measure the phosphorylation of ribosomal protein S6, a downstream target of the mTORC1-S6 kinase axis. As predicted, we discovered elevated phospho-S6 abundance in CD8$^+$ T cells cultured with FRCs relative to naïve T cells or those solely activated with anti-CD3/CD28 (Fig. 6a). Because increased S6 kinase activity promotes the biosynthesis of proteins, nucleotides and lipids, we compared de novo lipogenesis and neutral lipids in CD8$^+$ T cells from each condition. We found an increase in lipogenesis and accumulation of neutral lipids in CD8$^+$ T cells activated in the presence of FRCs (Fig. 6b,c), providing evidence for activation of lipid metabolism within CD8$^+$ T cells receiving signals from FRCs. Consistent with these findings, supplementation of our cultures with recombinant IL-6 augmented phospho-S6 levels and the accumulation of neutral lipids in activated CD8$^+$ T cells (Supplementary Fig. 4). We evaluated the metabolic flux of the cells in real time and found that the basal acidification rate (readout of glycolysis) and oxygen consumption rate (readout of mitochondrial respiration) were significantly increased in CD8$^+$ T cells activated in the presence of FRCs (Fig. 6d,e). Based on the ratio of basal oxygen consumption rate (OCR) to extracellular acidification rate (ECAR), FRC-conditioned CD8$^+$ T cells preferentially utilized OXPHOS for energy to a significantly greater degree than anti-CD3/CD28-activated CD8$^+$ T cells (Fig. 6f). It is important to note, however, that IL-2 can stimulate the induction of metabolic pathways in activated T cells[31]. Therefore, the observed promotion of T cell metabolism by FRCs or IL-6 may in part be due to the activity of IL-2. Nevertheless, these results demonstrate that FRC-derived signals markedly enhance the metabolic activity of activated CD8$^+$ T cells (Fig. 6g).

FRCs extend the longevity of CD8$^+$ T cells in vivo. To determine whether the gain of enhancer activity and gene expression in pro-survival and memory pathways is associated with increased T cell longevity, we investigated the survival potential of FRC-educated CD8$^+$ T cells in vitro and in vivo. To address this question in vitro, we activated whole splenocytes with anti-CD3/CD28 alone or in the presence of *Nos2*$^{-/-}$ FRCs for 48 h. CD8$^+$ T cells were then sorted from these cultures, allowed to rest in complete media for 72 h and subsequently assessed for viability based on uptake of propidium iodide. In accordance with our epigenetic and transcriptional signatures, FRC-educated CD8$^+$ T cells survived better (44-fold) than those activated only with anti-CD3/CD28 (Supplementary Fig. 5d). Given the equivalent viability of both T cell populations before sorting (Supplementary Fig. 5b), this result suggests that FRCs endow activated CD8$^+$ T cells with the ability to persist after removal of TCR and co-stimulation signals.

To determine whether signals from FRCs enhance the longevity of activated CD8$^+$ T cells in vivo, we utilized a competitive transfer system in which CD8$^+$ T cells specific for the peptide GP33-41 (P14 TCR transgenic) were activated in vitro with or without FRCs and then co-transferred into mice that were infected with influenza virus expressing GP33-41 (PR8-GP33) (Fig. 7a). Notably, following transfer and reactivation in animals infected with influenza, FRC-educated CD8$^+$ T cells persisted significantly better (20-fold, $P = 0.0003$) at day 8 post infection compared to T cells initially activated with only anti-CD3/CD28 (Fig. 7b). FRC-derived signals also offered a competitive advantage to T cells recovered from the lungs and spleen of animals infected with an acute strain of lymphocytic choriomeningitis virus (LCMV Armstrong) (Supplementary Fig. 5e,f). Of interest, this conditioning was durable as FRC-educated CD8$^+$ T cells survived better (18-fold, $P < 0.0001$) than their counterparts

Fig. 5 | FRCs or IL-6 amplify metabolic and survival pathways in activated CD8$^+$ T cells via epigenetic and transcriptional alterations. a, Heat map displaying enrichment (binomial test) of Gene Ontology (GO) terms (rows) in each module (columns) from Fig. 4e ($n = 3$ biologically independent cell cultures). **b**, Motif enrichment analysis comparing differential accessibility of transcription factor (TF) binding motifs in Act versus FRC condition (highlighted TFs, $P \leq 0.0008$, HOMER) ($n = 3$ biologically independent cell cultures). **c**, Enrichment of TF binding motifs in the FRC and IL-6 conditions compared to Act-only condition ($P \leq 0.01$, hypergeometric test) ($n = 3$ biologically independent cell cultures). **d**, Representative ATAC-seq tracks from each CD8$^+$ T cell condition in genes *Hk1* (top) and *Pfkfb3* (bottom) ($q < 0.001$ for FRC and IL-6 compared to Act) ($n = 3$ biologically independent cell cultures) **e**, Heat map showing replicate averaged gene expression of metabolic genes in the glycolysis pathway. ***$P = 0.0005$ (two-tailed Wilcoxon matched-pairs signed-rank test) ($n = 3$ biologically independent cell cultures (FRC) and 2 biologically independent cell cultures (Act and IL-6)). **f**, Representative ATAC-seq tracks from each CD8$^+$ T cell condition in genes *Bcl2* (top) and *Cflar* (bottom) ($q < 0.001$ for FRC and IL-6 compared to Act) ($n = 3$ biologically independent cell cultures). **g**, Heat map showing replicate averaged gene expression of representative pro-survival genes. *$P = 0.0156$ (two-tailed Wilcoxon matched-pairs signed-rank test) ($n = 3$ biologically independent cell cultures (FRC) and 2 biologically independent cell cultures (Act and IL-6)). Data represent one ATAC-seq and one RNA-seq experiment.

at 37 d post infection (Fig. 7c) and preferentially facilitated their differentiation into TRMs at 143 d post infection (Fig. 7d). To assess whether these differences were due to differing rates of proliferation, we pulsed the infected animals with BrdU and found that T cells activated with anti-CD3/CD28 proliferated to the same degree as FRC-educated T cells—suggesting that the observed longevity is due to enhanced survival potential (Supplementary Fig. 5g,h).

To determine whether IL-6 was necessary and sufficient for the induction of this enhanced longevity, we conducted similar in vivo competition assays with P14 T cells activated with anti-CD3/CD28 versus those activated with anti-CD3/CD28 plus recombinant IL-6. Recombinant IL-6 significantly enhanced (fivefold, $P = 0.0006$) the longevity of T cells in vivo (Fig. 7e) and facilitated their differentiation into TRMs at 160 d post infection (Fig. 7f). Importantly, when

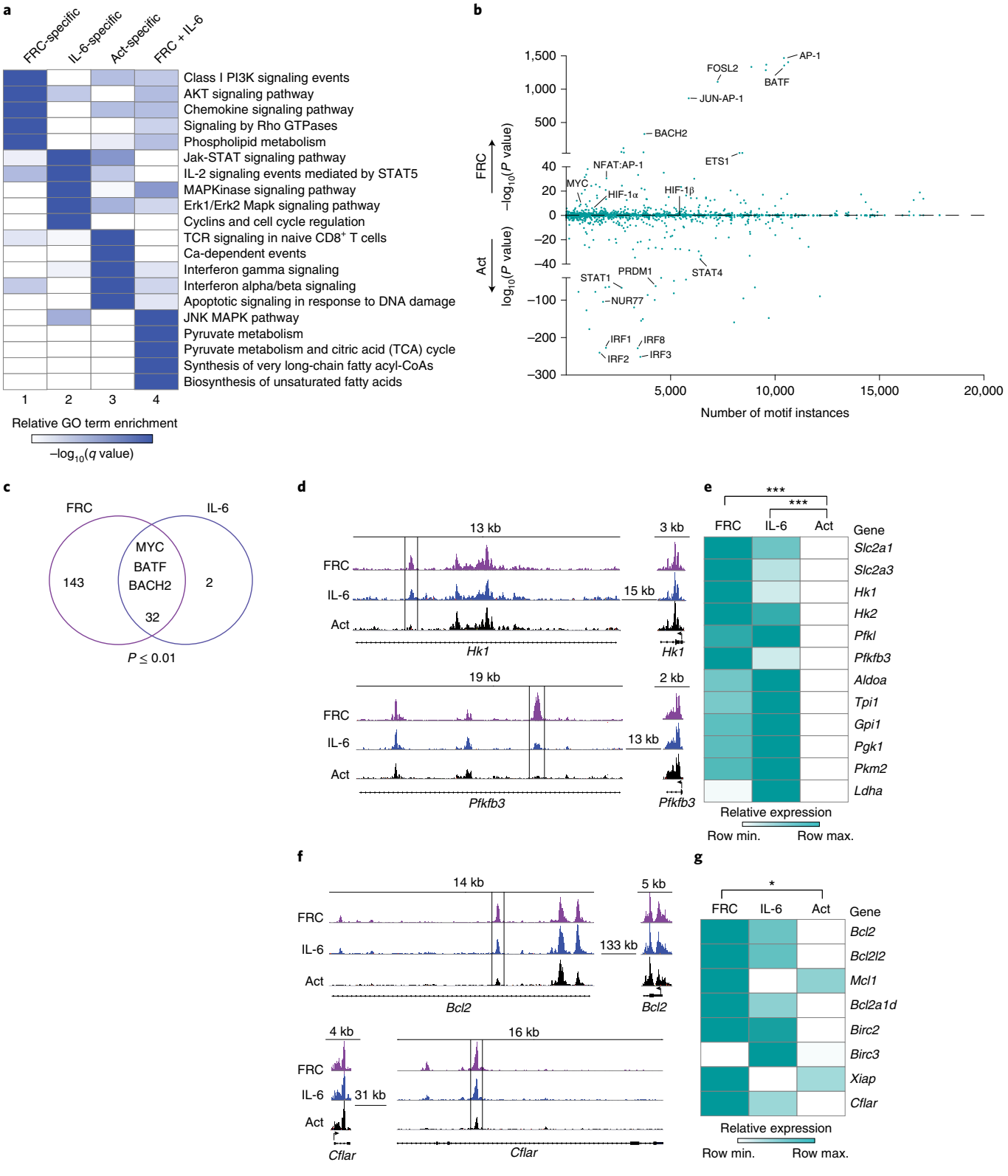

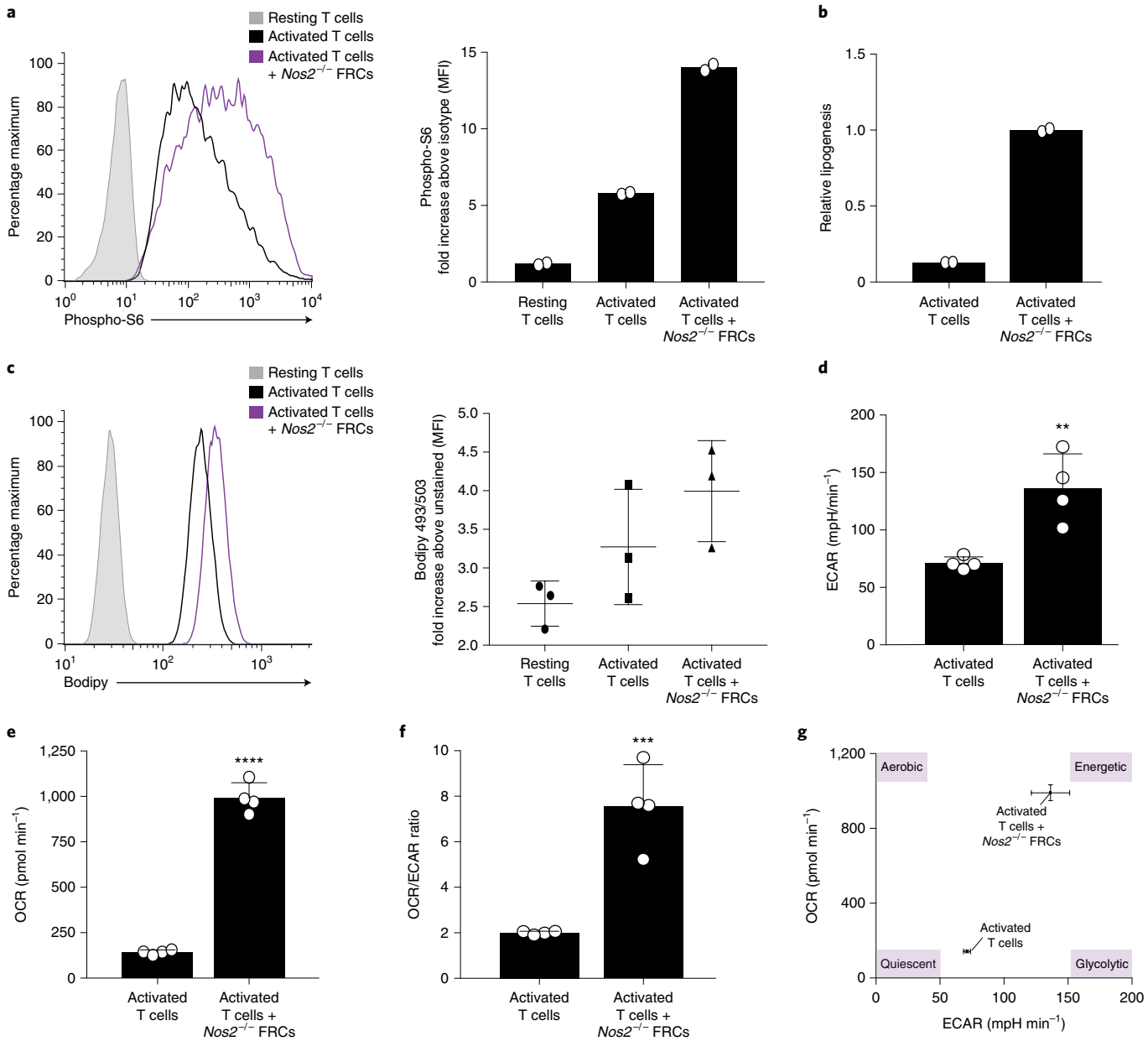

Fig. 6 | FRCs enhance the bioenergetic state of activated CD8⁺ T cells. a, Phospho flow cytometry of P-S6 levels in resting CD8⁺ T cells, those activated in whole-splenocyte mixtures via anti-CD3/CD28 for 48 h or activated via anti-CD3/CD28 for 48 h in the presence of *Nos2*$^{-/-}$ FRCs. Left, representative plot; right, summary ($n = 2$ biologically independent cell cultures per group). MFI, geometric mean fluorescence intensity. **b**, Relative de novo lipogenesis in CD8⁺ T cells either solely activated for 48 h with anti-CD3/CD28 or activated in the presence of *Nos2*$^{-/-}$ FRCs ($n = 2$ biologically independent cell cultures per group). **c**, Bodipy staining in CD8⁺ T cells under same conditions as **a**. Left, representative plot; right, summary ($n = 3$ biologically independent cell cultures per group). **d**–**f**, Basal ECAR $^{**}P = 0.0052$ (two-tailed Student's *t*-test), OCR $^{****}P < 0.0001$ (two-tailed Student's *t*-test) and OCR/ECAR ratio $^{***}P = 0.0009$ (two-tailed Student's *t*-test) in sorted CD8⁺ T cells following activation in whole-splenocyte mixture via anti-CD3/CD28 for 48 h or activation in the presence of *Nos2*$^{-/-}$ FRCs ($n = 4$ biologically independent cell cultures per group). mpH, milli-pH. **g**, Energy map comparing the global bioenergetic status of CD8⁺ T cells activated only with anti-CD3/CD28 versus those activated with anti-CD3/CD28 in the presence of *Nos2*$^{-/-}$ FRCs ($n = 4$ biologically independent cell cultures per group). Data in **a**–**c** are representative of two biologically independent experiments (mean ± s.d.); data in **d**–**g** are representative of two biologically independent experiments (mean ± s.d. (**d**–**f**), mean ± s.e.m. (**g**)).

we neutralized IL-6 in our FRC–T cell co-culture with anti-IL-6 blocking antibody before transfer, we found that T cells exposed to IL-6 significantly outcompeted (fivefold, $P < 0.0001$) those that did not receive IL-6-induced signals (Fig. 7g). Although neutralization of IL-6 led to a significant decrease in the absolute number of transferred cells producing IL-2 or TNF (Supplementary Fig. 6d), the frequency of cytokine-producing cells was not affected on a per-cell basis (Supplementary Fig. 6b,c), suggesting that FRC-derived IL-6 transiently regulates the production of cytokines in newly activated CD8⁺ T cells.

To evaluate the role of stromal cell-derived IL-6 in vivo, we monitored antiviral immunity in *Il6*$^{-/-}$ bone marrow chimeras (Supplementary Fig. 7a,b) responding to influenza infection. Since the hematopoietic system was the only source of IL-6 in these animals, we reasoned that this model would allow us to study the in vivo importance of IL-6 production specifically from

radioresistant cells such as FRCs. Among LN radioresistant stromal cells, we determined that FRCs are the most abundant and exhibit the highest per-cell production of IL-6 during an inflammatory response (Supplementary Fig. 7c,d). Importantly, compared to WT chimeric controls, these *Il6*$^{-/-}$ chimeras experienced enhanced weight loss and significantly delayed viral clearance during acute influenza infection (Fig. 7h). We assessed T cell persistence in the lungs of animals that successfully cleared the infection, and found a reduced frequency of antigen-experienced CD44^{+} and CD8^{+} T cells in *Il6*$^{-/-}$ chimeras compared to WT controls (Supplementary Fig. 7e). Altogether, these results suggest that stromal cell-derived IL-6, including FRC-originating, extends the longevity of virus-specific CD8^{+} T cells and regulates the overall efficiency of antiviral immunity.

Discussion

Lymph node FRCs exhibit several immunoregulatory functions, including controlling the activation of T lymphocytes[9]. After sensing IFN-γ and TNF, FRCs produce nitric oxide, which reduces the proliferation of activated T cells within close proximity[22–24]. Here, we have shown that FRCs also express immunostimulatory molecules in response to signals from activated T cells. FRC-derived IL-6, in particular, impacted multiple processes within activated CD8^{+} T cells. IL-6 enhanced production of IL-2 and TNF and altered chromatin accessibility in activated CD8^{+} T cells. Our studies suggest that these epigenetic changes facilitated differential TF activity—which seemed to promote metabolic reprogramming, survival and memory differentiation of CD8^{+} T cells.

Recent studies have shown that CD8^{+} T cells acquire changes within accessible chromatin that are enriched for specific TF binding motifs during their differentiation into effector and memory populations[42,44–46]. Here we demonstrate that FRC-derived signals, including IL-6, act in concert with TCR signaling and co-stimulation to remodel chromatin and render essential TF binding motifs accessible in CD8^{+} T cells. Signals from FRCs led to increased binding regions for MYC, HIF-1α and HIF-1β, which are known to promote metabolic pathways following T cell activation[34–36]. Accordingly, FRC-conditioned CD8^{+} T cells upregulated MYC- and HIF-1-dependent glycolysis genes and displayed enhanced glycolytic flux. Furthermore, FRC-conditioned T cells had a higher OCR/ECAR ratio—which demonstrates the preferred use of OXPHOS over glycolysis for energy generation. Importantly, FRC conditioning also increased de novo lipogenesis and amplified lipid storage programs. These features mirror the energy profile of in vitro-generated memory CD8^{+} T cells and viral-induced CD8^{+} TRMs, respectively[47,48]. Indeed, FRC signals, including IL-6, facilitated the differentiation of CD8^{+} T cells into TRMs during influenza infection. Collectively, our results suggest that FRC-derived signals drive metabolism-associated epigenetic changes that support CD8^{+} T cell survival and memory differentiation.

Additionally, FRC-derived signals promoted activity of TFs that regulate survival and memory programs in T lymphocytes. BATF is upregulated during CD8^{+} T cell differentiation and is required for their survival during infection[39,40]. Similarly, BACH2 is expressed in virus-specific CD8^{+} T cells and is necessary for primary responses and establishment of protective immunity[37]. We found an enrichment of binding motifs for BATF and BACH2 in FRC-conditioned T cells. Correspondingly, T cells harboring these enriched motifs exhibited a survival benefit both in vitro and in vivo. This heightened survival of FRC-conditioned T cells is similar to the consequences of BATF overexpression in virus-specific CD8^{+} T cells during infection[40]. Based on these observations, our motif analysis suggests that FRC-derived signals can support T cell survival and memory differentiation, in part by regulating the activity of BATF and BACH2.

Although FRCs expressed several immunostimulatory molecules in response to activated T cells, we focused on IL-6, which is known to elicit broad effects on innate and adaptive immune cells[49]. Our work highlights the ability of IL-6 to promote the bioenergetics, survival and differentiation of CD8^{+} T cells via alterations in chromatin accessibility. These data are consistent with previous studies which demonstrated a requirement of IL-6 for optimal CD8^{+} T cell responses against vaccinia, tuberculosis and influenza[50–52]. Notably, BATF expression in T cells is regulated by components of the IL-6 signaling pathway, including STAT3 (ref. [40]). This implies a potential IL-6–STAT3–BATF signaling axis in our system and further suggests a regulatory mechanism driven by differential TF activity. Though many stromal cell subsets and hematopoietic cells can produce IL-6, its cellular sources in the LN parenchyma during immune responses remain incompletely understood. In line with previous reports[26,27,53,54], we present herein a model where LN FRCs residing adjacent to T cells release IL-6 during T cell activation. This IL-6 would locally act on the expanding T cell pool to influence the ensuing response. Although IL-6 was sufficient to enhance T cell functions, its impact failed to fully replicate the stimulatory effect of intact FRCs, suggesting that FRCs produce additional T cell-enhancing factors.

Considering the inhibitory nature previously ascribed to FRCs[22–24,55,56], further work is needed to understand their role in promoting the functions of activated T lymphocytes. Our study took advantage of primary in vitro expanded cultures to clearly demonstrate that FRCs can express molecules with diverse immunological functions in response to signals from activated T cells. As such, FRCs were capable of inhibiting proliferation via NOS2 activity while also enhancing cytokine production, metabolic flux and survival via IL-6. How FRCs establish or maintain these seemingly

Fig. 7 | FRC-derived signals extend the longevity of virus-specific CD8^{+} T cells during influenza infection. a, Schematic diagram of competitive transfer system. **b**, Competitive frequencies of pre-activated P14 T cells as diagramed in **a** before transfer (Day 0) and 8 d following transfer into WT recipients infected with influenza. Top, representative plots; bottom, summary ($n = 5$ mice per group). ***$P = 0.0003$ (two-tailed ratio paired *t*-test). P.I., post influenza infection. **c**, Frequency of competitive mixes at Day 0 and 37 d post influenza infection. Top, representative plots; bottom, summary ($n = 8$ mice per group). ****$P < 0.0001$ (two-tailed ratio paired *t*-test). **d**, Absolute number of TRMs (CD69^{+} and CD103^{+}) within transferred P14 competitive mixes recovered from lungs 143 d after the onset of influenza infection. Top, representative plots; bottom, quantification of absolute numbers ($n = 7$ mice per group). **$P = 0.0023$ (two-tailed paired *t*-test). **e**, Competitive frequencies of P14 T cells activated in whole-splenocyte mixtures with anti-CD3/CD28 versus P14 T cells activated with anti-CD3/CD28 and 100 ng ml^{-1} recombinant IL-6. Top, representative plots; bottom, summary ($n = 5$ mice per group). ***$P = 0.0006$ (two-tailed ratio paired *t*-test). **f**, Absolute number of TRMs (CD69^{+} and CD103^{+}) within transferred P14 competitive mixes recovered from lungs 160 d after the onset of influenza infection. Top, representative plots; bottom, quantification of absolute numbers ($n = 5$ mice per group) **$P = 0.0022$ (two-tailed paired *t*-test). **g**, Competitive frequencies of P14 T cells activated in whole-splenocyte mixtures with anti-CD3/CD28 in the presence of *Nos2*$^{-/-}$ FRCs and 10 μg ml^{-1} anti-IL-6 blocking antibody versus P14 T cells activated under the same conditions with 10 μg ml^{-1} isotype control antibody. *Il6*$^{-/-}$ recipients were used for the transfers in **g**. Top, representative plots; bottom, summary ($n = 10$ mice per group) ****$P < 0.0001$ (two-tailed ratio paired *t*-test). **h**, Weight loss (top) and viral clearance (bottom) in WT and *Il6*$^{-/-}$ bone marrow chimeras on day 9 post influenza infection ($n = 10$ mice per group) *$P = 0.019$ (chi-squared test). Data in **b** and **g** are representative of three biologically independent experiments. Data in **c**–**f** are representative of two biologically independent experiments. Data in **h**, $n = 10$ mice per group, top panel shown as mean ± s.e.m.

divergent characteristics in vivo during an immune response remains unclear. Based on our data, we speculate that FRCs may exhibit functional heterogeneity during T cell priming in vivo. One piece of data supporting this notion comes from the in vivo expression profile of NOS2 in FRCs. As reported from the immunostaining of LNs, NOS2 expression was observed in only a proportion of

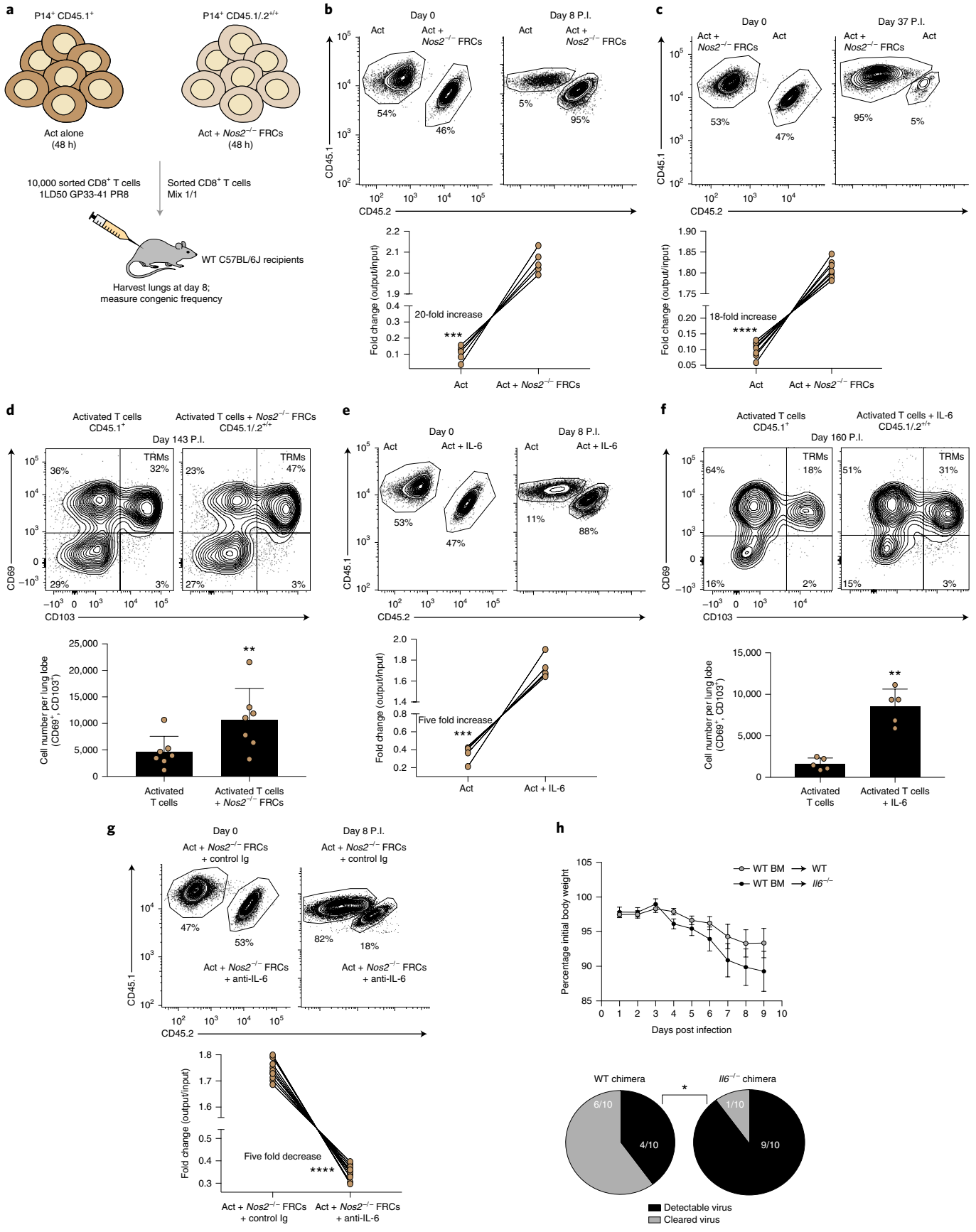

FRCs[22,23]. These results suggest that FRCs may have heterogeneous activity with regard to their regulation of immune cells. Indeed, functional heterogeneity of FRCs was described recently in regard to their ability to regulate B cell homeostasis[25] and antibody-secreting plasma cells[26,27]. Additionally, several new niche-specific subsets of LN stromal cells have been identified—all with potentially distinct functions[57]. Therefore, we envision distinct FRC subsets residing in discrete microdomains that differentially affect T cells during their activation and differentiation. Additional studies are needed to determine the breadth of functional heterogeneity in the FRC compartment. Further insights into the diverse immune functions of FRCs may inform the development of therapies to treat infections, cancer and autoimmune disorders.

Online content

Any methods, additional references, Nature Research reporting summaries, source data, statements of code and data availability and associated accession codes are available at https://doi.org/10.1038/s41590-019-0515-x.

Received: 12 October 2017; Accepted: 11 September 2019;
Published online: 21 October 2019

References

1. Mueller, S. N. & Germain, R. N. Stromal cell contributions to the homeostasis and functionality of the immune system. *Nat. Rev. Immunol.* **9**, 618–629 (2009).
2. Turley, S. J., Fletcher, A. L. & Elpek, K. G. The stromal and haematopoietic antigen-presenting cells that reside in secondary lymphoid organs. *Nat. Rev. Immunol.* **10**, 813–825 (2010).
3. Roozendaal, R. & Mebius, R. E. Stromal cell–immune cell interactions. *Annu. Rev. Immunol.* **29**, 23–43 (2011).
4. Malhotra, D. et al. Transcriptional profiling of stroma from inflamed and resting lymph nodes defines immunological hallmarks. *Nat. Immunol.* **13**, 499–510 (2012).
5. Malhotra, D., Fletcher, A. L. & Turley, S. J. Stromal and hematopoietic cells in secondary lymphoid organs: partners in immunity. *Immunol. Rev.* **251**, 160–176 (2013).
6. Luther, S. A., Vogt, T. K. & Siegert, S. Guiding blind T cells and dendritic cells: a closer look at fibroblastic reticular cells found within lymph node T zones. *Immunol. Lett.* **138**, 9–11 (2011).
7. Perez-Shibayama, C., Gil-Cruz, C. & Ludewig, B. Fibroblastic reticular cells at the nexus of innate and adaptive immune responses. *Immunol. Rev.* **289**, 31–41 (2019).
8. Alexandre, Y. O. & Mueller, S. N. Stromal cell networks coordinate immune response generation and maintenance. *Immunol. Rev.* **283**, 77–85 (2018).
9. Brown, F. D. & Turley, S. J. Fibroblastic reticular cells: organization and regulation of the T lymphocyte life cycle. *J. Immunol.* **194**, 1389–1394 (2015).
10. Fletcher, A. L., Acton, S. E. & Knoblich, K. Lymph node fibroblastic reticular cells in health and disease. *Nat. Rev. Immunol.* **15**, 350–361 (2015).
11. Chang, J. E. & Turley, S. J. Stromal infrastructure of the lymph node and coordination of immunity. *Trends Immunol.* **36**, 30–39 (2015).
12. Luther, S. A., Tang, H. L., Hyman, P. L., Farr, A. G. & Cyster, J. G. Coexpression of the chemokines ELC and SLC by T zone stromal cells and deletion of the ELC gene in the plt/plt mouse. *Proc. Natl Acad. Sci. USA* **97**, 12694–12699 (2000).
13. Bajenoff, M. et al. Stromal cell networks regulate lymphocyte entry, migration, and territoriality in lymph nodes. *Immunity* **25**, 989–1001 (2006).
14. Asperti-Boursin, F., Real, E., Bismuth, G., Trautmann, A. & Donnadieu, E. CCR7 ligands control basal T cell motility within lymph node slices in a phosphoinositide 3-kinase independent manner. *J. Exp. Med.* **204**, 1167–1179 (2007).
15. Worbs, T., Mempel, T. R., Bolter, J., von Andrian, U. H. & Forster, R. CCR7 ligands stimulate the intranodal motility of T lymphocytes in vivo. *J. Exp. Med.* **204**, 489–495 (2007).
16. Denton, A. E., Roberts, E. W., Linterman, M. A. & Fearon, D. T. Fibroblastic reticular cells of the lymph node are required for retention of resting but not activated CD8(+) T cells. *Proc. Natl Acad. Sci. USA* **111**, 12139–12144 (2014).
17. Schumann, K. et al. Immobilized chemokine fields and soluble chemokine gradients cooperatively shape migration patterns of dendritic cells. *Immunity* **32**, 703–713 (2010).
18. Marsland, B. J. et al. CCL19 and CCL21 induce a potent proinflammatory differentiation program in licensed dendritic cells. *Immunity* **22**, 493–505 (2005).
19. Link, A. et al. Fibroblastic reticular cells in lymph nodes regulate the homeostasis of naive T cells. *Nat. Immunol.* **8**, 1255–1265 (2007).
20. Acton, S. E. et al. Dendritic cells control fibroblastic reticular network tension and lymph node expansion. *Nature* **514**, 498–502 (2014).
21. Astarita, J. L. et al. The CLEC-2-podoplanin axis controls the contractility of fibroblastic reticular cells and lymph node microarchitecture. *Nat. Immunol.* **16**, 75–84 (2015).
22. Lukacs-Kornek, V. et al. Regulated release of nitric oxide by nonhematopoietic stroma controls expansion of the activated T cell pool in lymph nodes. *Nat. Immunol.* **12**, 1096–1104 (2011).
23. Siegert, S. et al. Fibroblastic reticular cells from lymph nodes attenuate T cell expansion by producing nitric oxide. *PloS ONE* **6**, e27618 (2011).
24. Khan, O. et al. Regulation of T cell priming by lymphoid stroma. *PloS ONE* **6**, e26138 (2011).
25. Cremasco, V. et al. B cell homeostasis and follicle confines are governed by fibroblastic reticular cells. *Nat. Immunol.* **15**, 973–981 (2014).
26. Zhang, Y. et al. Plasma cell output from germinal centers is regulated by signals from Tfh and stromal cells. *J. Exp. Med.* **215**, 1227–1243 (2018).
27. Huang, H. Y. et al. Identification of a new subset of lymph node stromal cells involved in regulating plasma cell homeostasis. *Proc. Natl Acad. Sci. USA* **115**, E6826–E6835 (2018).
28. Brown, G. C. Regulation of mitochondrial respiration by nitric oxide inhibition of cytochrome c oxidase. *Biochim. Biophys. Acta Bioenerg.* **1504**, 46–57 (2001).
29. Wink, D. A. et al. DNA deaminating ability and genotoxicity of nitric-oxide and its progenitors. *Science* **254**, 1001–1003 (1991).
30. Buenrostro, J. D., Giresi, P. G., Zaba, L. C., Chang, H. Y. & Greenleaf, W. J. Transposition of native chromatin for fast and sensitive epigenomic profiling of open chromatin, DNA-binding proteins and nucleosome position. *Nat. Methods* **10**, 1213–1218 (2013).
31. Buck, M. D., O'Sullivan, D. & Pearce, E. L. T cell metabolism drives immunity. *J. Exp. Med.* **212**, 1345–1360 (2015).
32. MacIver, N. J., Michalek, R. D. & Rathmell, J. C. Metabolic regulation of T lymphocytes. *Annu. Rev. Immunol.* **31**, 259–283 (2013).
33. Chang, C.-H. et al. Posttranscriptional control of T cell effector function by aerobic glycolysis. *Cell* **153**, 1239–1251 (2013).
34. Wang, R. N. et al. The transcription factor myc controls metabolic reprogramming upon T lymphocyte activation. *Immunity* **35**, 871–882 (2011).
35. Tyrakis, P. A. et al. S-2-hydroxyglutarate regulates CD8(+) T-lymphocyte fate. *Nature* **540**, 236–241 (2016).
36. Finlay, D. K. et al. PDK1 regulation of mTOR and hypoxia-inducible factor 1 integrate metabolism and migration of CD8(+) T cells. *J. Exp. Med.* **209**, 2441–2453 (2012).
37. Roychoudhuri, R. et al. BACH2 regulates CD8(+) T cell differentiation by controlling access of AP-1 factors to enhancers. *Nat. Immunol.* **17**, 851–860 (2016).
38. Li, Q. S., Eppolito, C., Odunsi, K. & Shrikant, P. A. Antigen-induced Erk1/2 activation regulates Ets-1-mediated sensitization of CD8+ T cells for IL-12 responses. *J. Leukoc. Biol.* **87**, 257–263 (2010).
39. Kurachi, M. et al. The transcription factor BATF operates as an essential differentiation checkpoint in early effector CD8(+) T cells. *Nat. Immunol.* **15**, 373–383 (2014).
40. Xin, G. et al. A critical role of IL-21-induced BATF in sustaining CD8-T-cell-mediated chronic viral control. *Cell Rep.* **13**, 1118–1124 (2015).
41. Gray, S. M., Amezquita, R. A., Guan, T. X., Kleinstein, S. H. & Kaech, S. M. Polycomb repressive complex 2-mediated chromatin repression guides effector CD8(+) T cell terminal differentiation and loss of multipotency. *Immunity* **46**, 596–608 (2017).
42. Sen, D. R. et al. The epigenetic landscape of T cell exhaustion. *Science* **354**, 1165–1169 (2016).
43. Portt, L., Norman, G., Clapp, C., Greenwood, M. & Greenwood, M. T. Anti-apoptosis and cell survival: a review. *Biochim. Biophys. Acta Mol. Cell Res.* **1813**, 238–259 (2011).
44. Scott-Browne, J. P. et al. Dynamic changes in chromatin accessibility occur in CD8(+) T cells responding to viral infection. *Immunity* **45**, 1327–1340 (2016).
45. Yu, B. F. et al. Epigenetic landscapes reveal transcription factors that regulate CD8(+) T cell differentiation. *Nat. Immunol.* **18**, 573–582 (2017).
46. Scharer, C. D., Bally, A. P. R., Gandham, B. & Boss, J. M. Cutting edge: chromatin accessibility programs CD8 T cell memory. *J. Immunol.* **198**, 2238–2243 (2017).
47. van der Windt, G. J. W. et al. Mitochondrial respiratory capacity is a critical regulator of CD8(+) T cell memory development. *Immunity* **36**, 68–78 (2012).
48. Pan, Y. D. et al. Survival of tissue-resident memory T cells requires exogenous lipid uptake and metabolism. *Nature* **543**, 252–256 (2017).
49. Hunter, C. A. & Jones, S. A. IL-6 as a keystone cytokine in health and disease. *Nat. Immunol.* **16**, 448–457 (2015).
50. Kopf, M. et al. Impaired immune and acute-phase responses in interleukin-6-deficient mice. *Nature* **368**, 339–342 (1994).
51. Ladel, C. H. et al. Lethal tuberculosis in interleukin-6-deficient mutant mice. *Infect. Immun.* **65**, 4843–4849 (1997).

52. Lauder, S. N. et al. Interleukin-6 limits influenza-induced inflammation and protects against fatal lung pathology. *Eur. J. Immunol.* **43**, 2613–2625 (2013).
53. Pasztoi, M. et al. Mesenteric lymph node stromal cell-derived extracellular vesicles contribute to peripheral de novo induction of Foxp3+ regulatory T cells. *Eur. J. Immunol.* **47**, 2142–2152 (2017).
54. Fletcher, A. et al. Reproducible isolation of lymph node stromal cells reveals site-dependent differences in fibroblastic reticular cells. *Front. Immunol.* **2**, 35 (2011).
55. Yu, M. et al. Fibroblastic reticular cells of the lymphoid tissues modulate T cell activation threshold during homeostasis via hyperactive cyclooxygenase-2/prostaglandin E-2 axis. *Sci. Rep.* **7**, 3350 (2017).
56. Knoblich, K. et al. The human lymph node microenvironment unilaterally regulates T-cell activation and differentiation. *PloS Biol.* **16**, 24 (2018).
57. Rodda, L. B. et al. Single-cell RNA sequencing of lymph node stromal cells reveals niche-associated heterogeneity. *Immunity* **48**, 1014–1028 (2018).
58. Subramanian, A. et al. Gene set enrichment analysis: a knowledge-based approach for interpreting genome-wide expression profiles. *Proc. Natl Acad. Sci. USA* **102**, 15545–15550 (2005).
59. Liberzon, A. et al. The molecular signatures database hallmark gene set collection. *Cell Syst.* **1**, 417–425 (2015).

Acknowledgements

This work was supported by the US National Institutes of Health (grant no. RO1 5R01DK074500 to S.J.T. and W.N.H.; no. P01AI108545 to A.H.S; no. T32 CA207021 to M.W.L) and by a Howard Hughes Medical Institute Gilliam Fellowship for Advanced Study (to F.D.B). We thank members of the Turley, Haining and Sharpe laboratories for scientific insights and discussions. We also thank A. E. Mayfield for critical reading of the manuscript.

Author contributions

F.D.B. conceived and conducted most of the experiments, analyzed and interpreted data and wrote the manuscript. D.R.S. conducted experiments and analyzed and interpreted data. J.G., M.W.L., V.L.-K., F.A.S., H-J.K., K.B.Y., S.J.H.R., K.B. and V.N.K. conducted experiments and interpreted data. J.D.T. and I.A.S. discussed data and provided technical assistance. V.C., N.N.D. and B.D.M. discussed and interpreted data. A.H.S., W.N.H. and S.J.T. directed the study, analyzed and interpreted results and wrote the manuscript.

Competing interests

V.N.K. and S.J.T. are employees of Genentech. W.N.H. is an employee of Merck. V.C. is an employee of Novartis. F.D.B. is an employee of Neon Therapeutics. The authors declare no competing interests.

Additional information

Supplementary information is available for this paper at https://doi.org/10.1038/s41590-019-0515-x.

Correspondence and requests for materials should be addressed to A.H.S., W.N.H. or S.J.T.

Peer review information L. A. Dempsey was the primary editor on this article and managed its editorial process and peer review in collaboration with the rest of the editorial team.

Reprints and permissions information is available at www.nature.com/reprints.

Publisher's note Springer Nature remains neutral with regard to jurisdictional claims in published maps and institutional affiliations.

Methods

Mice. C57BL/6 (WT) male mice were purchased from Jackson Laboratory or Taconic. B6.129S2-*Il6*^{tm1Kopf}/J (*Il6*$^{-/-}$) and B6.129P2-*Nos2*^{tm1Lau}/J (*Nos2*$^{-/-}$) male mice were purchased from Jackson Laboratory. B6.129S2-*Nos2*^{tm1Mrl} N12 (*Nos2*$^{-/-}$) male mice were purchased from Taconic. P14 TCR transgenic mice were previously described[60]. C57BL/6-Tg(TcraTcrb)1100Mjb/J (OT-1) male mice were purchased from Jackson Laboratory. All male mice were used at 5–12 weeks of age. For infectious experiments, mice were housed in a specific pathogen-free barrier facility and used in accordance with animal care guidelines from the Harvard Medical Area Standing Committee on Animals and the National Institutes of Health. All other animals were maintained in specific pathogen-free facilities at the Dana-Farber Cancer Institute and were approved by the Animal Care and Use Committee of the Dana-Farber Cancer Institute.

Antibodies and flow cytometry. The following antibodies were used: anti-CD275 (HK5.3), anti-CD40 (3/23), conjugated and LEAF purified anti-IL-6 (MP5-20F3), anti-IL-2 (JES6-5H4), anti-CD8α (53-6.7), anti-CD8β (53-5.8) anti-TNF (MP6-XT22), anti-IFN-γ (XMG1.2), anti-CD45.1 (A20), anti-CD45.2 (104), anti-Thy1.1 (OX-7), anti-CD25 (PC61), anti-CD69 (H1.2F3), anti-CD103 (2E7), anti-CD45 (30-F11), anti-CD31 (MEC13.3), anti-CD16/32 (93), anti-CD44 (IM7), anti-CD11b (M1/70), anti-CD19 (6D5), anti-CD4 (RM4-5) and anti-podoplanin (8.1.1) (all from BioLegend); anti-CD140a (APA5; eBioscience) and anti-MHC class II (2G9) (both BD Biosciences). Functional-grade purified anti-CD3ε (145-2C11) was obtained from BD Biosciences, and anti-CD28 (37.51) from eBioscience. GP33 H-2Db Dextramers were obtained from Immudex, and L-NMMA (NG-monomethyl-L-arginine) was obtained from Calbiochem. Recombinant IL-6 was acquired from BioLegend. Intracellular staining for IL-6, IFN-γ, IL-2 and TNF was performed using an Intracellular Fixation and Permeabilization Buffer Set (eBioscience) following the addition of Brefeldin A during the final 4 h of T cell activation. For detection of phosphorylated S6 protein (P-S6), activated splenocytes were harvested, pretreated with Fc-blocking antibodies (anti-CD16/32) and stained for surface antigens CD8α and MHC-II (accessory cell exclusion) to gate on activated CD8$^+$ T cells. The cells were then fixed, permeabilized and stained for intracellular P-S6 (D57.2.2E) in accordance with Cell Signaling Technologies' phospho flow cytometry protocol. To measure neutral lipids, activated splenocytes were incubated in Fc-blocking antibodies, stained for surface antigens, washed with PBS and subsequently incubated in PBS with 10 μM BODIPY 493/503 (4,4-difluoro-1,3,5,7,8-pentamethyl-4-bora-3a,4a-diaza-s-indacene, Invitrogen) in the dark for 30 min at 37 °C. The cells were then washed with PBS and analyzed. Dilution of 5- (and -6) carboxyfluorescein diacetate, succinimidyl ester (CFSE) from Invitrogen was used to measure T cell proliferation. For some experiments, the incorporation of BrdU was measured 8 d after the onset of influenza infection in adoptively transferred P14 T cells to study T cell proliferation in vivo. Animals were treated with 2 mg BrdU (Sigma-Aldrich) intraperitoneally 10–12 h before analysis. BrdU incorporation was assessed by the BrdU Flow Kit according to the manufacturer's instructions (BD Biosciences). To sort activated CD8$^+$ T cells from co-cultures, activated splenocytes were harvested, Fc blocked and stained with surface antigens CD8α and MHC-II. Sorted CD8α$^+$ and MHC-II$^-$ cells were used in downstream applications. For FRC sorting, cells were briefly trypsinized and sorted from co-cultures using previously described gating strategies[54]. FACSAria (BD Biosciences) was used for analysis and sorting. Dead cells were excluded with propidium iodide staining solution (eBioscience). For enumeration of cells, CountBright Absolute Counting Beads for flow cytometry (Thermo Fisher, no. C36950) were used.

Co-culture of activated T cells and FRCs. Lymph nodes were digested and LN stromal cells were expanded ex vivo as previously described[22]. FRCs were purified as previously noted[22] and plated in 24-well-plates at 5×10^4 cells per well. To induce T cell activation, 1×10^6 splenocytes were added to each well the following day with soluble anti-CD3 (0.25 μg ml^{-1}) and anti-CD28 (0.25 μg ml^{-1}). The cultures were analyzed either 24 or 48 h later. For stimulation with plate-bound anti-CD3, 96-well round-bottomed plates were coated for 2–4 h at 37 °C with anti-CD3 (10 μg ml^{-1}) and washed once with PBS. Then, 4×10^4 FRCs and 1×10^5 purified CD8$^+$ T cells were added to the wells at the same time in the presence of soluble anti-CD28 (0.25 μg ml^{-1}). Cultures were analyzed 24 h later. For some experiments, CFSE-labeled (0.5 μM) splenocytes were used and analyzed 48 or 72 h later. Nitric oxide concentrations in co-culture supernatants were measured as previously described[22]. Purified CD8$^+$ T cells were obtained using the CD8a$^+$ T Cell Isolation Kit, mouse (no. 130-104-075), according to the manufacture's guidelines (Miltenyi).

RNA isolation and microarray hybridization. Fibroblastic reticular cells were briefly trypsinized and sorted from cultures as previously described[4]. RNA was isolated from cell pellets using the Qiagen RNeasy Mini kit according to the manufacturer's instructions. Extracted RNA was amplified and prepared for hybridization to the Mouse Genome 430 2.0 GeneChip using the Ovation RNA Amplification System V2 Assay, in accordance with the manufacturer's instructions. The arrays were scanned using GeneChip Scanner 3000 7 G.

Microarray analysis. Before analysis, mouse microarray data were normalized using the robust multiarray averaging method with background correction. To identify genes differentially expressed between resting FRCs and those cultured in the presence of activated T cells, differential expression analysis was performed using the linear modeling and empirical Bayesian method implemented in the limma R package (Bioconductor). Gene-set enrichment analysis was performed as described previously[58,59], using the C2 KEGG and Reactome collections of canonical pathway gene-sets from the MSigDB database. Gene-sets were considered differentially enriched at $P<0.05$ and $q<0.1$.

Metabolic flux of activated CD8$^+$ T cells. Activated CD8$^+$ T cells were sorted from cultures 44–48 h post activation and loaded onto the XF-24 or XF-96 Extracellular Flux Analyzer (Seahorse Bioscience) according to the manufacturer's instructions. OCR and ECAR were measured in XF media (nonbuffered RPMI or DMEM containing 25 mM glucose, 2 mM L-glutamine and 1 mM sodium pyruvate). The XF cell mito stress test kit was used to induce changes in flux in response to 1 μM oligomycin, 1–2 μM carbonyl cyanide 4-(trifluoromethoxy) phenylhydrazone and 0.5 μM rotenone/antimycin A.

Adoptive transfers and infections. Congenically marked, pre-activated P14 CD8$^+$ T cells were sorted from cultures 44–48 h post activation, mixed 1/1 (5×10^3 each) and transferred via the tail vein into WT or *Il6*$^{-/-}$ recipients. Directly after transfer, the animals were infected with either influenza or LCMV Armstrong. For influenza infections, 6–12-week-old mice were anesthetized with 2.5% Avertin (Sigma-Aldrich) and infected intranasally with PR8-GP33-41 (1LD50). For some experiments, mice were infected intraperitoneally with 2×10^5 plaque-forming units of LCMV Armstrong. The frequency of transferred cells was determined in the lungs and spleen of infected animals at various time points after the onset of infection. For some experiments, BrdU incorporation was assessed or the transferred cells were stained with CD69 and CD103 to evaluate the frequency of developed TRMs. Recombinant influenza virus containing the LCMV GP33-41 epitope was provided by R. Webby (St. Jude Children's Research Hospital, Memphis, TN, USA)[61,62]. LCMV Armstrong virus was provided by E. J. Wherry (University of Pennsylvania, Philadelphia, PA, USA). Viral titers in lungs were determined by quantitative real-time PCR (RT–qPCR) as described[61]. For some experiments, transferred cells were re-challenged in vitro with gp33 peptide (KAVYNFATC) for 6 h in the presence of Brefeldin A, followed by ICS staining to measure cytokine production.

Generation of bone marrow chimeras. C57BL/6J (WT) or *Il6*$^{-/-}$ hosts received two doses of 450–500 rads, 4 h apart. After the second irradiation, the mice received $6–10\times10^6$, ACK-lysed, whole bone marrow cells intravenously from CD45.1$^+$ WT donors. The animals were bled 6–12 weeks later to confirm hematopoietic reconstitution and used for subsequent experimentation.

Immunizations. OT-1 T cells (1×10^6) were transferred intravenously into C57BL/6J mice. Recipients were then immunized in the hind footpad with 500 μg ovalbumin (Sigma-Aldrich) in complete Freund's adjuvant (InvivoGen). For IL-6 ICS, immunized mice were injected intravenously with 100 μg Brefeldin A (eBioscience) 4–5 h before being sacrificed. LNs were digested as previously described[22], and single-cell suspensions were incubated in Brefeldin A for an additional 2 h. Intracellular staining for IL-6 was performed using an Intracellular Fixation and Permeabilization Buffer Set (eBioscience).

De novo lipid synthesis. Activated CD8$^+$ T cells were sorted from cultures 44–48 h post activation and incubated at 37 °C for 4 h with 6.6 μCi ml^{-1} 1-^{14}C-acetate (NEC084H001MC, Perkin Elmer). Cells were washed twice with PBS and then lysed in 0.5% Triton X-100. Lipids were extracted with 2/1 (v/v) chloroform/methanol (500 μl) and then centrifuged at 1,000 r.p.m. for 15 min. A LS6500 scintillation counter (Beckman Coulter) was used to quantify ^{14}C-labeled lipid in the denser fraction. Lipid quantification was normalized to protein concentration or cell number.

ATAC-seq preparation. A total of 50,000 CD8$^+$ T cells was activated in vitro for 48 h with anti-CD3/CD28 (Act), with or without recombinant IL-6 (Act + IL-6), or activated with anti-CD3/CD28 in the presence of FRCs (Act + FRCs) and sorted into PBS with 10% FBS. Pelleted cells were lysed in 50 μl of reaction mix (25 μl of 2× tagmentation DNA buffer, 2.5 μl of Tn5 enzyme, 0.25 μl of 2% digitonin and 22.25 μl of nuclease-free water) as previously described[63]. The reaction was incubated at 37 °C for 30 min with agitation at 300 r.p.m. DNA was purified using a QIAgen MinElute Reaction Cleanup kit, and Nextera sequencing primers ligated using PCR amplification. Agencourt AMPure XP bead cleanup (Beckman Coulter/Agencourt) was used post PCR and library quality was verified using a Tapestation machine. Samples were sequenced on an Illumina HiSeq 2000 sequencer using paired-end 5-base pair (bp) reads.

ATAC-seq analysis. Raw reads in Fastq files were trimmed for quality, and primers were removed using Trimmomatic-0.33 with the following parameters: LEADING, 15; TRAILING, 15; SLIDINGWINDOW, 4:15; MINLEN, 36. FastQC

reports were generated before and after trimming to assess quality. Trimmed reads were aligned to mm9 with Bowtie v.2.2.4 using a maximum insert size of 2,000. Aligned bam files were sorted for marking duplicates, and reads mapping to the blacklist region were removed[30,64]. Reads were shifted +4 and −5 bp using pysam 0.9.0 as previously described[30]. Bam files from biological replicates were merged using samtools 1.3 before peak-calling using MACS 2.1.1 at $q = 0.001$. Consensus peaks from the three biological conditions ($CD8^+$ T cells from Act, Act + IL-6 and Act + FRCs) were merged to create a single peak universe. Shifted cut sites were extracted from each biological replicate and the number of cuts within each peak region was quantified to generate a raw counts matrix. DESeq2 was used to normalize the counts matrix and perform differential accessibility analysis between all pairwise comparisons. Overlap of ChARs from each biological condition with published histone mark CHIP-seq data[39] was quantified using the hypergeometric ratio. Tracks were visualized using Integrative Genomics Viewer (Broad Institute). Gene-to-peak associations were determined using the GREAT software package (http://bejerano.stanford.edu/great/public/html/) with default settings. *K*-means clustering was applied using GENE-E (Broad Institute) to differential ChAR signal intensity across the three cell states. GENE-E was also used for heat map visualization and distance matrix calculations (Pearson). Principal component analysis was performed using R v.3.3.1. Motif enrichment analysis was performed using HOMER v.3.0. Genomic sequences corresponding to all peaks in the peak universe were extracted using bedtools v.2.17.0 and divided into three categories for FRC versus Act analysis—sequences corresponding to peaks that were upregulated in FRC ($q < 0.001$), sequences corresponding to peaks that were upregulated in Act ($q < 0.001$) and sequences corresponding to nondifferential peaks. HOMER motif enrichment was run on FRC- and Act-upregulated peaks using default settings and the set of nondifferential peaks as the background set. Gene Ontology term enrichment was performed for each biological condition using GREAT, with default settings and the Binomial test. ATAC-seq profiles corresponding to naive, effector and memory T cells from ref. [42] were compared to the FRC, IL-6 and Act conditions. bedtools (v.2.27.1) was used to generate ChAR overlaps, and the hypergeometric fold enrichment of each sample was calculated separately for the three categories of naive, effector and memory. For comparison to datasets from ref. [41], mm9-mapped ChARs were mapped to the mm10 genome alignment using the UCSC liftover tool. H3K4me3 peaks identified in naive, terminal effector and memory precursor cells in ref. [41] were overlapped with the FRC, IL-6 and Act conditions using BEDtools. Hypergeometric fold enrichment was calculated as above.

RNA-seq preparation and analysis. RNA was isolated as described above, and first-strand Illumina-barcoded libraries were generated using the NEB RNA Ultra Directional kit according to the manufacturer's instructions, including 12 cycles of PCR enrichment. Libraries were subsequently sequenced on an Illumina NextSeq 500 instrument using paired-end 37-bp reads. Trimmomatic pipeline was used to trim data for quality with the following parameters: LEADING, 15; TRAILING, 15; SLIDINGWINDOW, 4; 15 MINLEN, 16. Bowtie2 was used to align data to mouse mm10. HTSeq was used to map aligned reads to genes and to generate a gene count matrix. Technical failure during processing led to the exclusion of samples during analysis. DESeq2 was used to normalize the counts for library depth and perform differential expression analysis between all pairwise comparisons.

Data analysis and statistics. Flow cytometry data were analyzed using FlowJo v.10.2 software. Unless otherwise noted, Prism v.7.0 (GraphPad Software) was used to conduct unpaired, two-tailed *t*-tests, with 95% confidence intervals (Student's *t*-test) and the assumption of equal sample variance. For competitive adoptive transfer experiments, a two-tailed paired or ratio paired *t*-test was used. A chi-squared test was used to assess viral clearance in bone marrow chimeric mice. A two-tailed Wilcoxon matched-pairs signed-rank test was used to compare gene expression within glycolysis and pro-survival pathways between samples. Statistics for RNA-seq and ATAC-seq were performed using DESeq2.

Reporting Summary. Further information on research design is available in the Nature Research Reporting Summary linked to this article.

Data availability

All data that relate to or support the observations described in this study are available from the corresponding authors upon reasonable request. The ATAC-seq and RNA-seq data have been deposited in the Gene Expression Omnibus (GEO) database under accession no. GSE136905. The Microarray data are accessible through GEO accession no. GSE136958.

References

60. Pircher, H., Burki, K., Lang, R., Hengartner, H. & Zinkernagel, R. M. Tolerance induction in double specific T-cell receptor transgenic mice varies with antigen. *Nature* **342**, 559–561 (1989).
61. Laidlaw, B. J. et al. Cooperativity between CD8+ T cells, non-neutralizing antibodies, and alveolar macrophages is important for heterosubtypic influenza virus immunity. *PloS Pathog.* **9**, e1003207 (2013).
62. Mueller, S. N. et al. Qualitatively different memory CD8+ T cells are generated after lymphocytic choriomeningitis virus and influenza virus infections. *J. Immunol.* **185**, 2182–2190 (2010).
63. Corces, M. R. et al. Lineage-specific and single-cell chromatin accessibility charts human hematopoiesis and leukemia evolution. *Nat. Genet.* **48**, 1193–1203 (2016).
64. Dunham, I. et al. An integrated encyclopedia of DNA elements in the human genome. *Nature* **489**, 57–74 (2012).